Geostatistical Estimation of Resolution-Dependent Variance in Remotely Sensed Images

John B. Collins and Curtis E. Woodcock

Abstract

The variance of a remotely sensed image is determined by the interaction of scene properties with the spatial characteristics of the sensor. Image variance is related to information content, and therefore determines the ability to extract useful information about scene conditions. We describe a technique to estimate image variance at multiple spatial resolutions. The method is useful for comparing the capabilities of sensors with differing spatial responses.

The point-spread function (PSF) and the variogram quantify the spatial characteristics of the sensor and image, respectively. A geostatistical model based on these two elements relates the punctual variogram of a scene with the regularized variogram of an image. This model forms the basis for a numerical approach to approximate the punctual variogram from regularized observations. The resulting estimate of the punctual variogram allows analytical determination of image variance at different spatial resolutions.

Analysis of simulated images confirms the utility of this algorithm. Variance of coarse-resolution images may be estimated reliably from fine-resolution data. Simulations of multiscale variability show that the method handles more complex types of scene variability as well. The geostatistical variance estimation algorithm better characterizes the relationship between variance and spatial resolution than do simpler methods, such as averaging blocks of pixels. Specifically, methods which do not account for overlap of adjacent placements of the sensor PSF tend to overestimate the variance of the resulting images. The algorithm presented here can be used to evaluate the utility of different sensors for particular applications, when the relationship between spatial resolution and image information content is important.

Introduction

Investigations of scale dependence in digital images often focus on changes in information content as a function of the spatial interval over which measurements are taken. *Information content* is associated with the second-order properties of an image, including the variance and autocovariance function. These properties are influenced by all components of the underlying scene, including the spatial arrangement of scene objects, their spectral properties, variability in atmospheric conditions, and view and illumination angles. The measurement interval, or *measurement scale*, is associated with sensor spatial resolution. The effect of measurement scale on the amount and quality of information which can be extracted from a digital image is recognized as a fundamental issue in remote sensing (Quattrochi and Goodchild, 1997).

Woodcock and Strahler (1987) present relationships between spatial resolution and mean local variance of image data at different scales. The spatial resolution at which local variance reaches a maximum is considered closely to match the characteristic scale of scene variation. The latter study and others (Markham and Townshend, 1981; Cushine, 1987) discuss the relevance of resolution-dependent effects to the accuracy of multispectral image classification. Specifically, spatial resolution determines the relative variability between and within land-cover classes, influencing spectral separability. Marceau *et al.* (1994a; 1994b) use the resolution dependence of classification accuracy to assess optimum spatial resolutions for feature extraction.

Friedl *et al.* (1995) and Friedl (1997) describe the use of a scene simulation model to investigate the precision with which biophysical properties can be inverted from remotely sensed data. This precision is shown to depend on sensor characteristics. Hu and Islam (1997) present a model which explicitly relates the error of such biophysical models to the variance of the input data, which is determined by the spatial resolution.

Many studies of scale dependence take an empirical approach in which a multiresolution data set is created by aggregating successively larger blocks of fine-resolution pixels (Chou, 1991; Wielicki and Parker, 1992; Peuch, 1994; Qi and Wu, 1996; Hay *et al.*, 1997). Empirical analysis of a small number of scenes is useful if the data set at hand is the primary object of analysis, for example, if one wishes to characterize the spatial properties of a particular geographic area. However, empirical analysis gives only limited insights into the scaling properties of spatial data in general. Results of any analysis only have widespread utility if the conditions under which they apply can be stated explicitly. These conditions are difficult or impossible to define by analysis of a particular scene.

Additionally, creating coarse-resolution data by averaging blocks of fine-resolution pixels is, at best, a rough approximation of the way in which remote sensing devices operate. Remotely sensed measurements are not simple averages of radiance within a sensor's field of view, and this field of view may not be rectangular (as is often implicitly assumed when averaging pixels). Instead, sensor optical and electronic effects cause scene radiance to be weighted differently according to its relative spatial position. The way in which a sensor weights scene radiance when making a measurement is described by the sensor's point spread function (PSF) (or equivalently, by its frequency-domain representation, the modulation transfer function). Using a simple averaging process is equivalent to assuming that the PSF has the

Boston University Department of Geography, 675 Commonwealth Avenue, Boston, MA 02215.

J.B. Collins is presently at Atmospheric and Environmental Research, 840 Memorial Drive, Cambridge, MA 02139.

Photogrammetric Engineering & Remote Sensing, Vol. 65, No. 1, January 1999, pp. 41–50.

0099-1112/99/6501–0041$3.00/0

form of a simple square wave. Few if any studies have explicitly assessed the impact of modeling the remote sensing process using such assumtions.

This article takes a more deterministic approach to the problem of relating image variance to sensor spatial properties. We describe a model of the relationship between image variance and sensor spatial resolution which explicitly identifies the relevant components of the sensor and of the scene. Making use of the sensor PSF implies that the remote sensing process can be modeled as a shift-invariant linear system, in which a measurement of scene radiance is obtained by a convolution process. This is still an approximation to the true operation of remote sensing devices, but it is an improvement over methods based on averaging blocks of pixels. In addition to the spatial properties of the sensor (as measured by the PSF), the other relevant consideration is the spatial structure of the scene. The latter can be summarized by its autocovariance function or variogram. The variogram has been applied extensively in analysis of remotely sensed images (Woodcock *et al.*, 1988a; Woodcock *et al.*, 1988b; Curran, 1988; Jupp *et al.*, 1988; Jupp *et al.*, 1989). The key element of the model to be discussed here is the geostatistical theory of regularization, which describes the way in which statistical properties of data are affected by the measurement process.

In the remote sensing context, the sensor PSF is associated with the geosatistical notion of *support*, or interval over which measurements are made. Predictable relationships between variance and support size have long been noted (Smith, 1938). In fact, determination of such relationships is a standard problem in geostatistics (Jupp *et al.*, 1989; Zhang *et al.*, 1990) and in analysis of random fields (Vanmarcke, 1983). Graphs illustrating such relationships are often called *auxiliary functions*, and have been tabulated by several authors (for example, Rendu (1978)). This article reviews these results with emphasis on identifying the support with the PSF of a remote sensing device. The observations, variance, and variogram are said to be *regularized*. This term distinguishes the measured quantities from the underlying properties of the scene, which are said to be *punctual* (i.e., occurring at the scale of points rather than over finite areas).

Theoretical results indicate how the variance and variogram of punctual data are modified by a sensor PSF. These relationships lead to an algorithm to estimate the punctual variogram from regularized observations. The problem has been addressed by Atkinson and Curran (1995), making use of developments in Journel and Huijbregts (1978). A similar approach is presented in this article. Furthermore, a simple relationship between punctual and regularized variance relates the regularized variance of two different images of the same scene. The basic mathematical results leading to these analysis techniques are well-known. But this particular combination of approaches — estimating the punctual variogram and relating the variance of two different images of the same scene — allows the use of a single observation to characterize the statistical properties of observations made by different sensors. An image simulation study is presented in order to investigate the conditions under which the algorithm produces acceptable results. The algorithm has potential applications in modeling studies to determine required spatial resolutions for particular applications.

Linear Systems and Statistical Image Models

A remotely sensed image can be modeled as the output of a shift-invariant linear system. The radiance sensed at a point t in an image $Y(t)$ is the convolution of scene radiance $Z(t)$ with the system point spread function $r(u)$ (Rosenfeld and Kak, 1982): i.e.,

$$Y(t) = \int_u r(u)\, Z(t - u)\, du. \tag{1}$$

All parameters are vectors representing position in two-dimensional space. Such a convolution integral can also be written $[Z * r](t)$. In geostatistics, the spatially varying radiance $Z(t)$ is modeled as a realization of a regionalized variable. The field $Z(t)$ and the output $Y(t)$ have second-order properties described by their autocovariance functions $\kappa_Z(h)$ and $\kappa_Y(h)$, respectively. The two are related as follows (Vanmarcke, 1983, p. 107):

$$\kappa_Y(h) = \int_{u'}\int_v r(u')\, r(v)\, \kappa_Z(h + u' - v)\, dv\, du'. \tag{2}$$

A more convenient form results from the change of variables $u = u' + h$: i.e.,

$$\kappa_Y(h) = \int_u \int_v r_h(u)\, r(v)\, \kappa_Z(u - v)\, dv\, du. \tag{3}$$

The function $r_h(u) \equiv r(u - h)$ is a translation of the PSF $r(u)$ by the vector h.

The variogram is a more familiar tool in remote sensing than is the autocovariance function. One may derive a relationship between the variograms of the input and output processes corresponding to the relationship for autocovariance functions in Equation 3. Using the identity $\gamma_Y(h) = \kappa_Y(0) - \kappa_Y(h)$ and substituting Equation 3 for κ_Y gives

$$\gamma_Y(h) = \int_u \int_v r(u)\, r(v)\, \kappa_Z(u - v)\, dv\, du - \int_u \int_v r_h(u)\, r(v)\, \kappa_Z(u - v)\, dv\, du. \tag{4}$$

Making the substitution $\kappa_Z(u - v) = \kappa_Z(0) - \gamma_Z(u - v)$ and noting that terms involving $\kappa_Z(0)$ cancel gives the result

$$\gamma_Y(h) = \int_u \int_v r_h(u)\, r(v)\, \gamma_Z(u - v)\, dv\, du - \int_u \int_v r(u)\, r(v)\, \gamma_Z(u - v)\, dv\, du. \tag{5}$$

Each of the terms on the right is an average of variogram values at lag $u - v$, weighted by the product $r_h(u)\, r(v)$ (for the first term) and by $r(u)\, r(v)$ (for the second term). The notation adopted for integrals of this form will be

$$\int_u \int_v f(u)\, g(v)\, \gamma_Z(u - v)\, dv\, du \equiv \overline{\gamma}_Z(f, g). \tag{6}$$

Similar notation has been used elsewhere to denote average variogram values between two supports and between individual points and supports (Webster *et al.*, 1989; Atkinson and Curran, 1995). Equation 5 can be written as

$$\gamma_Y(h) = \overline{\gamma}_Z(r_h, r) - \overline{\gamma}_Z(r, r). \tag{7}$$

This relates the variograms of the input and output processes with the system PSF. This result has been shown by other authors for the case in which r is an indicator function representing membership in a support (Rendu, 1978). The above derivation indicates that results are similar when one specifically considers the spatial weighting characteristics of the PSF.

Variance of Linear Processes

The variance of the output process $Y(t)$ is the value of its autocovariance function at a lag of zero, which can be related to the autocovariance function of Z by Equation 3: i.e.,

$$\sigma_Y^2 = \kappa_Y(0) = \int_u \int_v r(u)\, r(v)\, \kappa_Z(u - v)\, dv\, du. \tag{8}$$

Once again, making use of the identity relating κ_Z and γ_Z,

$$\sigma_Y^2 = \int_u \int_v r(u)\, r(v)\, \kappa_Z(0)\, dv\, du - \int_u \int_v r(u)\, r(v)\, \gamma_Z(u - v)\, dv\, du. \quad (9)$$

Using the fact that $\kappa_Z(0) = \sigma_Z^2$, the definition $\int_u r(u)\, du \equiv |r|$, and Equation 6, this becomes

$$\sigma_Y^2 = \sigma_Z^2\, |r|^2 - \overline{\gamma}_Z(r, r). \quad (10)$$

Suppose a second remotely sensed image is made of $Z(s)$. Denote this as

$$X(t) = [Z * s](t), \quad (11)$$

where $s(u)$ is the PSF of the system producing $X(t)$. The variance of this process is given by Equation 10: i.e.,

$$\sigma_X^2 = \sigma_Z^2\, |s|^2 - \overline{\gamma}_Z(s, s). \quad (12)$$

Combining Equations 10 and 12 shows

$$\sigma_X^2 = \frac{|s|^2}{|r|^2} \{\sigma_Y^2 + \overline{\gamma}_Z(r, r) - \overline{\gamma}_Z(s, s)\}. \quad (13)$$

If both PSFs are normalized to have unit volume, the $|s|^2/|r|^2$ term drops out of Equation 13. This result gives the relationship between the variance of two different processes created by convolution of the same input process with different PSFs. If two satellite images with different spatial resolutions (and hence different PSFs) are made of the same scene, Equation 13 shows how their variances are related to each other, and to the underlying spatial structure of the scene.

An Algorithm for Punctual Variogram Estimation

Equation 10 shows that the regularized variance of the output process depends on $\gamma_Z(h)$, the punctual variogram of the input process. For a given application, if a model of the punctual variogram is available or may be assumed, Equation 10 may be used directly for determination of variance for any image with a known PSF. Such a punctual variogram may be available if, for example, measurements are made on supports small enough to be considered points. A regularized variogram, however, corresponding to $\gamma_Y(h)$, may be the only available information on the image's spatial structure. Some approximation to the punctual variogram must be derived from the regularized data.

Variograms used in practice are mathematical models fit to observed values. A number of standard models meet the requirement of being conditionally negative semi-definite. Two such models are the exponential

$$\gamma(h) = c[1 - e^{-h/a}] \quad (14)$$

and the spherical

$$\gamma(h) = \begin{cases} c\left[\frac{3h}{2a} - \frac{h^3}{2a^3}\right] & h < a \\ c, & h \geq a \end{cases}. \quad (15)$$

Each model has two parameters, the *sill* c and the *range* a. The sill is the value which the variogram approaches at large lags, and the range is related to the lag at which the sill is reached, or the distance within which observations are correlated. In the following discussion, it will be necessary to specify the form and parameters of arbitrary variogram models. For this purpose, the notation Exp(c, a) will denote an exponential variogram model with sill c and range a. The notation Sph(c, a) will denote a spherical model.

To determine a functional form for the variogram, the typical approach is to choose a model or sum of models based on intuition or experience as to which form is most appropriate. Then one optimizes the fit between the model and observations with respect to the variogram parameters. This fit can be described by the sum of squared deviations, or by more complicated weighting schemes (Cressie, 1985). Denote a vector of parameters λ, and a resulting variogram model as $\gamma_Y(h; \lambda)$ (i.e., the inclusion of the parameter λ indicates a modeled quantity). Assuming that the fit of the model is evaluated by a sum of squared differences, one finds a value for λ which minimizes

$$\sum_{i=1}^{n} [\gamma_Y(h_i, \lambda) - \hat{\gamma}_Y(h_i)]^2, \quad (16)$$

where $\hat{\gamma}_Y(h_i)$ is a variogram value estimated from the available data, and n is the number of lags h_i for which the variogram is calculated.

Numerical methods can be used to determine a model for the *punctual* variogram $\gamma_Z(h, \lambda)$ directly from the regularized data $\hat{\gamma}_Y(h)$. Approaches to the problem have been presented by Atkinson and Curran (1995) and by Collins and Woodcock (1996). These methods are based on (1) fitting a model to regularized observations, then (2) adjusting the parameters of an assumed punctual model until its regularization closely matches the model fitted to the data. The approach described here is similar, but does not require initial fitting of a model to observations.

Equation 7 is the key to determining a punctual model directly from regularized observations. Given a model punctual variogram, its counterpart regularized by the PSF r is

$$\gamma_Y(h; \lambda) = \overline{\gamma}_Z(r_h, r; \lambda) - \overline{\gamma}_Z(r, r; \lambda). \quad (17)$$

The punctual model is determined by the value for λ which minimizes the difference between this *regularized model* and the *regularized observations* $\hat{\gamma}_Y(h_i)$: i.e.,

$$\sum_{i=1}^{n} [\gamma_Y(h_i, \lambda) - \hat{\gamma}_Y(h_i)]^2. \quad (18)$$

These developments allow estimation of a punctual variogram and, hence, estimation of image variance at arbitrary spatial resolutions, based on analysis of a single image. Data required for input to the algorithm are (1) a remotely sensed image, (2) the PSF of the sensor used to create the image, and (3) the PSF for a sensor whose image variance is to be estimated.

Applications of Variance Estimation

The algorithm presented above relies on numerical approximation of the punctual variogram from regularized observations. Because numerical approximations are not exact solutions, the performance of the algorithm should be checked. Image simulation is an ideal tool for preliminary analysis of algorithm performance because it allows concentration on image and sensor spatial attributes, while ignoring extraneous differences to be expected in actual remotely sensed images (Kerekes and Landgrebe, 1989). Certain qualities of actual images, however, are important for this type of analysis. So following assessment of algorithm performance employing simulated images, an example based on an actual image is presented.

Image Simulation

A set of simulated images was created by first generating a grid of autocorrelated values, then degrading it by convolution with a series of PSFs. The punctual data were generated on a grid of 1024 by 1024 points, at a nominal spacing of one meter. (Note the distinction between punctual data at a spacing of one meter and regularized data at a one-meter resolution.) The simulated values were calculated by a two-di-

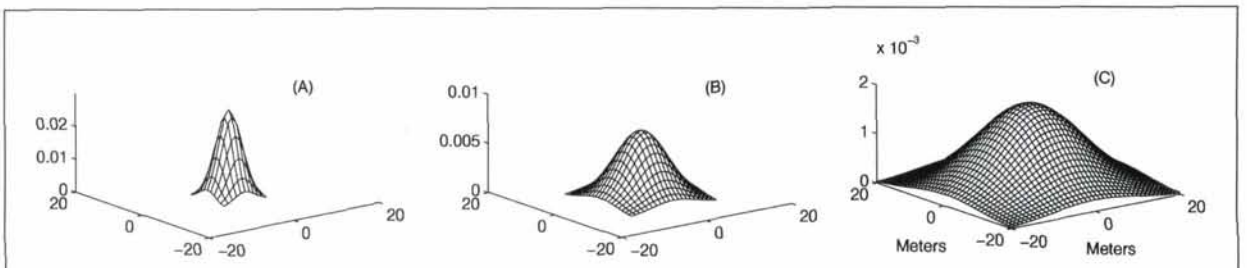

Figure 1. Gaussian Point Spread Functions for spatial resolutions of (A) 5 meters, (B) 10 meters, and (C) 20 meters, all normalized to have unit volume. Note the change of scale of the vertical axis.

mensional autoregressive process simulator, summarized by the following formula:

$$Z(x, y) = \Re\{F^{-1}[F[N(x, y)] \cdot f(j, k)]\}, \quad (19)$$

where $Z(x, y)$ is the simulated value at spatial location (x, y), F and F^{-1} are the forward and inverse Fourier transform operators, respectively, $N(x, y)$ is a grid of unit-variance normally distributed random numbers, and $f(j, k)$ is a frequency response function of a point (j, k) in frequency space. $\Re$ denotes selection of the real part of a complex number. The frequency response function is parameterized such that the resulting process exhibits spatial autocorrelation. Specifically, its value is

$$f(j, k) = \frac{1}{1 - 2a[\cos\frac{2\pi j}{n} + \cos\frac{2\pi k}{n}]}. \quad (20)$$

Here, n is the dimension of the image (1024 in this case), and a is the parameter controlling the degree of autocorrelation. The value of a is constrained to the interval [0, 0.25), with larger values implying greater autocorrelation. A value of $a = 0.2495$ was used to simulate the punctual data. Pixel values were scaled to the arbitrary range of (0, 100).

Images were created by a discrete approximation to the convolution integral (Equation 1). That is, the PSF model was sampled at a nominal one-meter spacing, to match the sampling interval of the simulated data. This approach causes smaller PSFs to be sampled with less relative density than larger ones. But for even the smallest PSF used here, this results in a sample of 121 points (on an 11 by 11 grid), which is sufficient to characterize the PSF's shape.

The PSF of a remote sensing system is actually a combination of PSFs associated with several system components, such as lenses, detectors, and amplifiers. The combination of PSFs is usually approximated well by a Gaussian function (Billingsley *et al.*, 1983): i.e.,

$$r(x, y) = K \exp\left\{-\frac{x^2 + y^2}{2R^2}\right\}. \quad (21)$$

The "radius" of the function is given by the parameter R. In this study, we identify the spatial resolution of the simulated sensor as the diameter ($2R$) of the PSF. The factor K is determined by the system gain. When processing remotely sensed data, however, one usually accounts for the system gain by converting digital counts to at-sensor radiances. In such a case, K can be taken to equal 1. Examples of PSFs of 5 meters, 10 meters, and 20 meters are shown in Figure 1. In all cases, the PSFs were constrained to the interval $-2R \le x \le 2R$, $-2R \le y \le 2R$. That is, the full width of a PSF model is twice its nominal resolution. This accounts for radiance integrated from outside the sensor's nominal field of view. Images created by convolving modeled PSFs with the punctual data are shown in Figure 2.

Variance Estimation from Simulated Images

For an initial validation of the algorithm, the 5-meter data served as the base from which variance at all other resolutions was estimated. The 5-meter data were used to estimate the punctual variogram (Figure 3). Values of the regularized variogram were calculated from the data to a lag of 100 meters, and are shown in the graph. The sill and the range of a spherical variogram model were determined by minimizing the sum of squared differences between the observed variogram and the variogram as regularized by a 5-meter Gaussian PSF. The punctual variogram shown in Figure 3 is given by $\gamma(h) = \text{Sph}(152, 39.5)$. There is no particular closed-form expression for the corresponding regularized model, because it is calculated using Equation 7. Also shown in Figure 3 are values of the punctual variogram determined from the 1-meter data. The numerical procedure succeeded in choosing parameters for the punctual variogram such that when it is regularized, the resulting function closely matches observed values. However, this close match does not imply as close a match between the punctual model and the punctual data. The punctual sill is slightly overestimated, and the estimated range is too small.

Using this punctual model, variance was estimated for all spatial resolutions of the simulated data, assuming a Gaussian PSF for the regularized images (Figure 4). The variances for the 5-meter data match by definition. For the remaining resolutions, variance is estimated with reasonable precision. The relatively close match between the observed and estimated variances, in spite of errors in estimation of the punctual variogram, indicates that the algorithm is robust with respect to the punctual variogram parameters. Clearly, the magnitude of the error evident in Figure 3 does not cause serious errors in variance estimation. The relatively large discrepancy between observed and estimated variance for the 100-meter data may be due to the small number of pixels available for calculating variance at this spatial resolution.

Figure 5 illustrates attempts to estimate the punctual variogram from the 10-meter, 20-meter, and 50-meter images. Results become increasingly worse as spatial resolution becomes coarse. Estimation of the punctual variogram from the 10-meter data is fairly precise ($\gamma(h) = \text{Sph}(147, 39.4)$), but use of either the 20-meter data ($\gamma(h) = \text{Sph}(130, 49.0)$) or the 50-meter data ($\gamma(h) = \text{Sph}(78, 81.3)$) results in unacceptably large errors. Figure 6 shows the effect of such erroneous estimates. For the 10-meter data, estimation of variance at all resolutions is acceptable. Both of the coarser spatial resolutions result in incorrect estimates for finer resolutions, with the magnitude of the error proportional to the error in estimation punctual parameters. But in both cases, estimates at coarse resolutions remains precise.

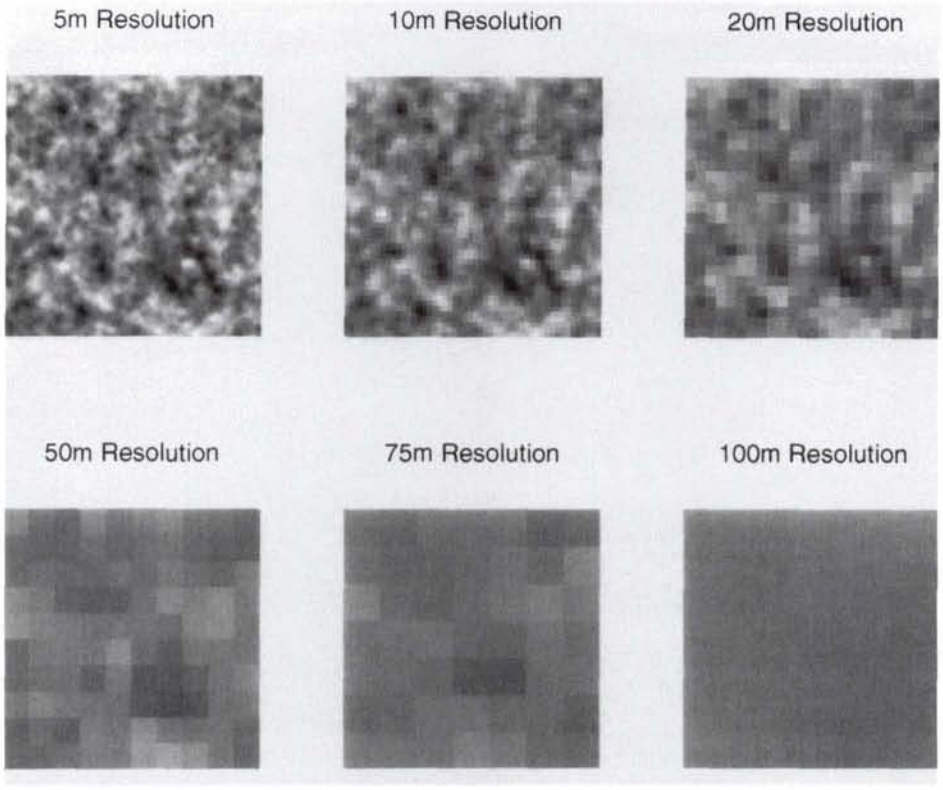

Figure 2. Images simulated by convolution of punctual data with Gaussian PSFs. Nominal spatial resolutions are 5, 10, 20, 50, 75, and 10 meters.

The simulated scene in Figure 2 has a fairly simple structure. In an attempt to investigate the utility of the variance estimation algorithm for more complex scenes, a multiscale scene was simulated (Figure 7). To create the multiscale scene, single-scale images were calculated using three different values of the autocorrelation parameter a. The three component images were summed, and the resulting image was scaled to the range [0, 100]. As is shown in Figure 8, the variance estimation algorithm is able to deal with the extra spatial complexity. This figure suggests that knowledge of the regularized variogram allows estimation of resolution-dependent variance regardless of the spatial structure of the underlying scene.

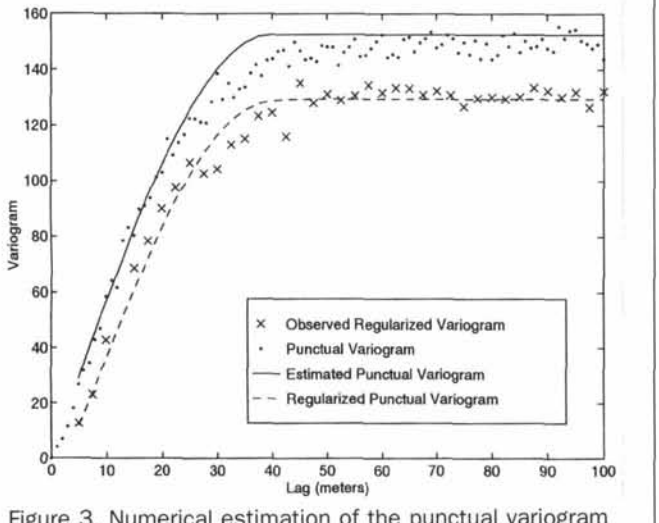

Figure 3. Numerical estimation of the punctual variogram $\gamma_Z(h)$ from 5-meter regularized data. Punctual variogram data are shown for reference.

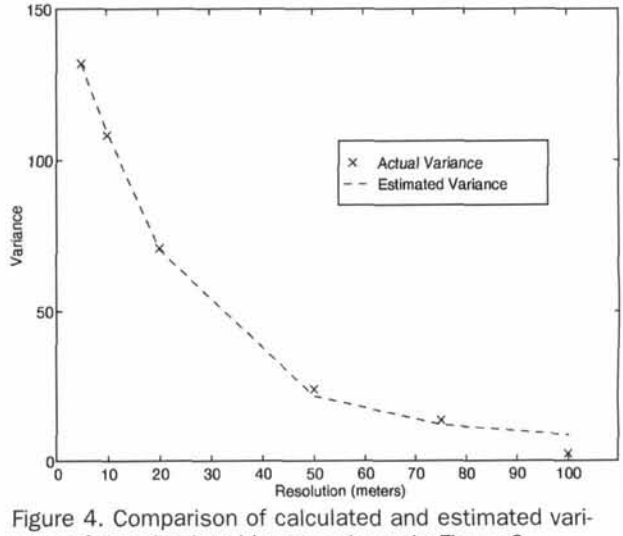

Figure 4. Comparison of calculated and estimated variance of the simulated images shown in Figure 2.

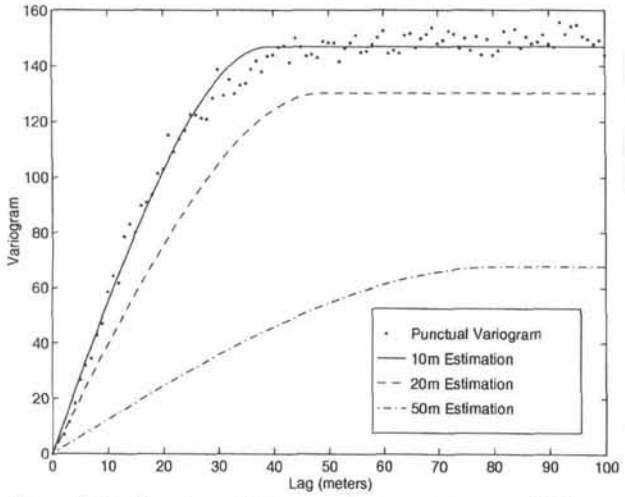

Figure 5. Estimation of the punctual variogram $\gamma_Z(h)$ from 10-, 20-, and 50-meter data. Punctual variogram data are shown for reference.

Comparison With Other Approaches

The algorithm for estimating variance for arbitrary sensors with Gaussian PSFs is both complex and computationally expensive. Examination of possible alternatives is worthwhile. The computational cost of the algorithm may be reduced by assuming a simpler model for the sensor PSF. Specifically, a PSF can be modeled as an indicator-type function, for example, a disk (Figure 9). Another alternative to the algorithm outlined above is to degrade a fine-resolution image by averaging blocks of pixels, and then to calculate the variance of the degraded image.

A comparison of such alternative approaches is presented in Figures 10 and 11. Figure 10 shows attempts to estimate the punctual variogram from the 5-meter image (Figure 2) by assuming a disk model. Results are fairly good — at least no worse than results obtained from assuming a Gaussian PSF. The variogram model shown in the figure is $\gamma(h) = \text{Sph}(142, 41.6)$, very close to the estimate obtained using the Gaussian PSF model ($\gamma(h) = \text{Sph}(147, 39.4)$). Figure 11, on the other hand, shows that estimation of variance at other resolutions by these alternative approaches is problematic. Using a disk PSF, or estimating variance by block averaging, results in overestimation of the variance of the degraded images. Also shown in Figure 11 is the expected variance for a white-noise process for which variance is inversely proportional to spatial resolution. This curve corresponds to estimated variance under the assumption that the data have no spatial structure. Results for the random case plot as a straight line on double logarithmic plots, as shown

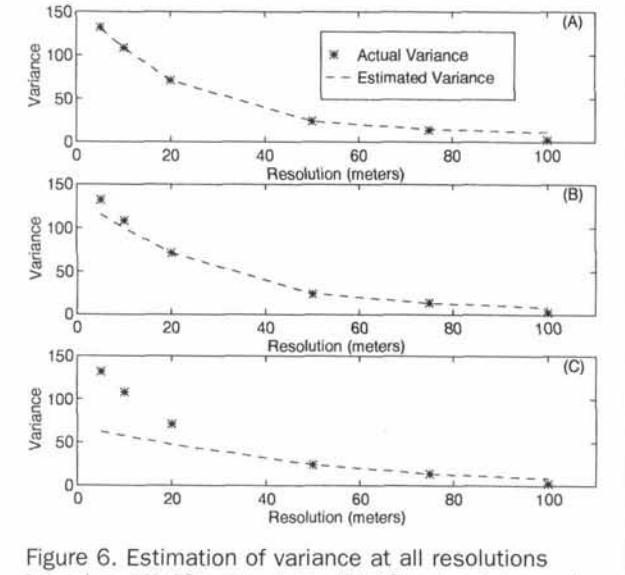

Figure 6. Estimation of variance at all resolutions based on (A) 10-meter data, (B) 20-meter data, and (C) 50-meter data.

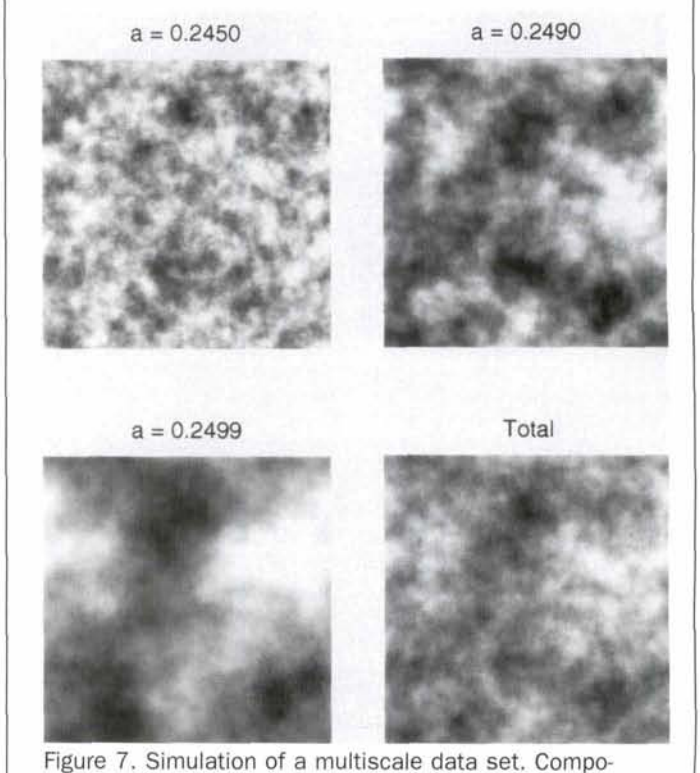

Figure 7. Simulation of a multiscale data set. Components created using three different values of the autocorrelation parameter (a) were added in order to produce a multiscale scene.

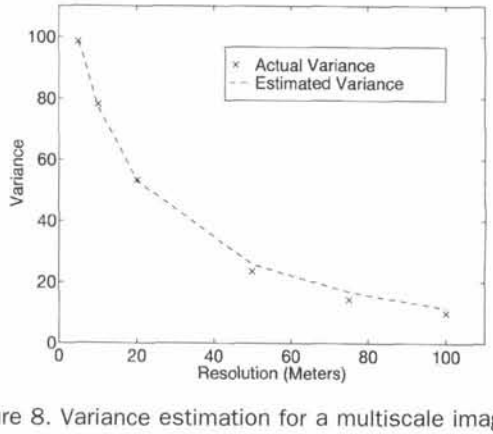

Figure 8. Variance estimation for a multiscale image.

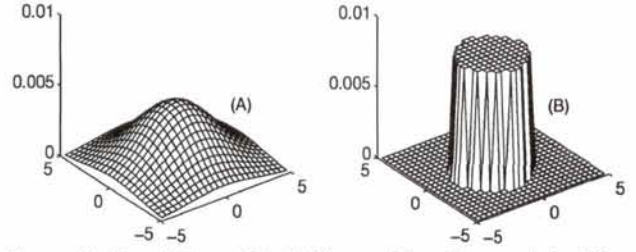

Figure 9. Two different Point Spread Function models. (A) Gaussian model. (B) Disk model. Both PSFs have a nominal spatial resolution of 5 meters.

in the lower portion of the figure. Contrasts between curves in the lower plot highlight the effects of spatial structure.

Another alternative is to use a frequency-domain approach to determining variance as a function of sensor PSF. Consider two images $X(t)$ and $Y(t)$ which are functions of a spatial variable t. These images may be considered convolutions of a scene $Z(t)$ with some PSF: i.e.,

$$X(t) = [Z * r](t), \qquad Y(t) = [Z * s](t). \tag{22}$$

The convolution theorem (Jenkins and Watts, 1968) states that the Fourier transform of an image becomes the product of the Fourier transform of the two functions involved in the convolution: i.e.,

$$FX(\omega) = FZ(\omega)\, Fr(\omega), \qquad FY(\omega) = FZ(\omega)\, Fs(\omega). \tag{23}$$

In these equations, FX denotes the Fourier transform of X, parameterized by the spatial frequency ω. Combining these equations and solving for FY shows that

$$FY(\omega) = \frac{Fs(\omega)}{Fr(\omega)}\, FX(\omega). \tag{24}$$

So, given an image $X(t)$, its PSF $r(t)$, and the PSF $s(t)$ of another image $Y(t)$, one can determine the frequency-domain representation of Y. The important implication is that the variance of an image can be determined directly from its transform, as follows:

$$\sigma_Y^2 = \sum_{\omega} |FY(\omega)|^2. \tag{25}$$

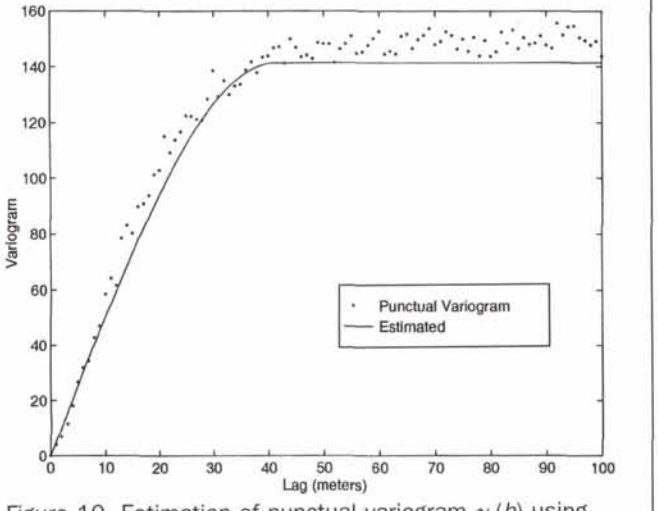

Figure 10. Estimation of punctual variogram $\gamma_Z(h)$ using the disk PSF model. The estimation is based on the 5-meter image shown in Figure 2.

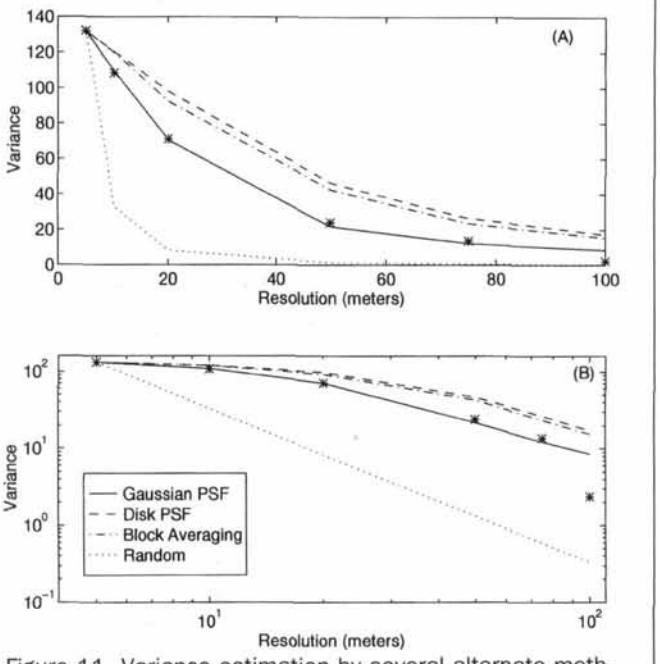

Figure 11. Variance estimation by several alternate methods. The lower portion shows the same information as the top portion, using logarithmic scaling.

The method outlined above was applied to the simulated data shown in Figure 2. The results, shown in Figure 12, indicate that the method performs well. Its level of accuracy is comparable to that obtained using variograms, which indicates that the approaches essentially make use of equivalent information.

Analysis of Real Images — An Example

Analysis of simulated images confirms the theory behind the variance estimation algorithm. But analysis of real scenes raises a number of important issues. Figure 13 shows part of a Landsat TM scene, Band 3 (0.63 to 0.69 μm). The image, taken on 16 August 1985, shows a conifer forest in Oregon. The area covered by this image is subject to frequent logging, and the bright patches are recent clearcuts. It is possible to use the spatial information contained in this image to estimate how much information (variance) would be present for such a scene in images of other spatial resolutions.

Figure 14 shows the image variogram. A qualitative difference between this variogram and those observed for simulated data is the presence of a small nugget variance. The model shown in Figure 14 is $\gamma(h) = 4.05 + \mathrm{Exp}(31.1, 211)$, where 4.05 is the nugget. Atkinson (1997) argues that a nugget effect in remotely sensed data is due to measurement error, and should be discarded. Such action could be taken in this example, because measurement error for the original image does not affect estimated variance for other sensors.

The nugget effect in Figure 14 was subtracted, and the resulting zero-nugget variogram was used to estimate the punctual variogram, assuming a 30-meter Gaussian PSF. Figure 15 shows estimated variance for other sensors with Gaussian PSFs of various spatial resolutions. Even at fairly coarse resolutions of about 300 meters, roughly half of the variance

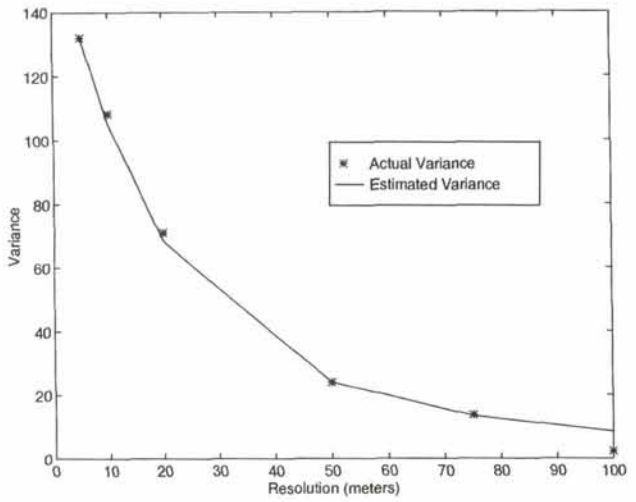

Figure 12. Variance estimation based on the Fourier transform of the 5-meter image data.

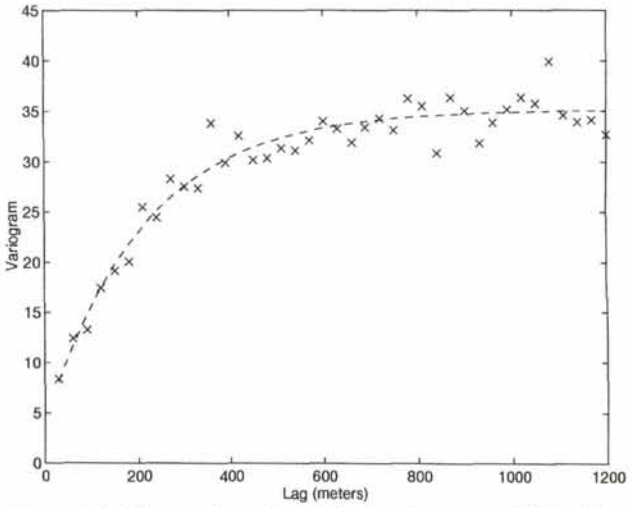

Figure 14. Observed and modeled variograms $\gamma(h)$ for the test image. The observed variogram is indicated by the 'x' marks, and the model is shown by the dashed line.

obtained at 30 meters could be expected. This is apparently due to the relatively large size of objects in this scene, and the large range of the observed variogram. Because the nugget effect of the target sensors is not included, the plotted values represent what the variance of such a scene would be in the absence of sensor noise.

Discussion

Algorithm Performance

Variance estimation for simulated images was highly successful, in spite of the fact that an intermediate step — estimation of the punctual variogram — is error-prone. A possible explanation lies in Equation 13. This Equation contains the difference between the average variogram for two PSFs, one associated with the original image and the other associated with a sensor whose attributes are to be described. Both averages are calculated from a punctual model $\gamma_Z(h, \lambda)$. So errors in the estimate of $\gamma_Z(h, \lambda)$ cause errors of similar magnitudes for both $\overline{\gamma}_Z(r, r)$ and $\overline{\gamma}_Z(s, s)$. Taking the difference of these two quantities tends to minimize the error. This is not to say that arbitrary values could be chosen for the punctual variogram parameters. On the contrary, the approach assures that punctual parameters are such that the variogram at a 30-meter resolution is estimated correctly. Information at the original scale, and presumably at coarser scales, is preserved.

There is nothing inherent in the algorithm to prevent es-

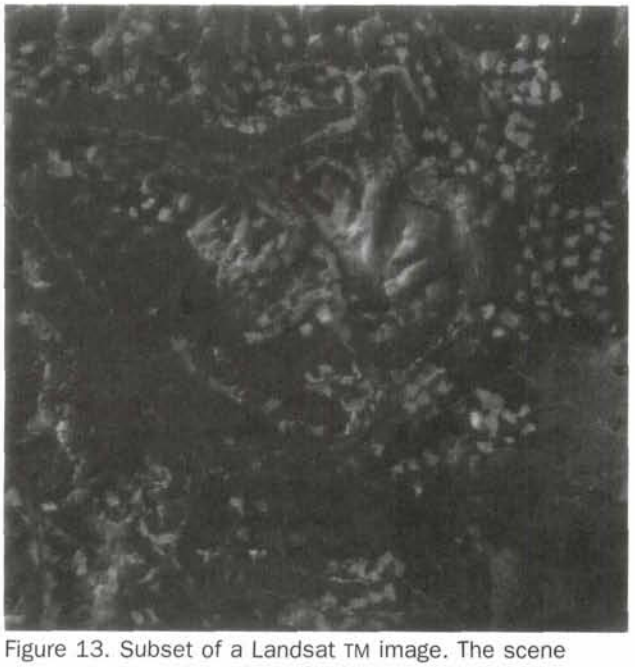

Figure 13. Subset of a Landsat TM image. The scene measures approximately 24 by 24 km.

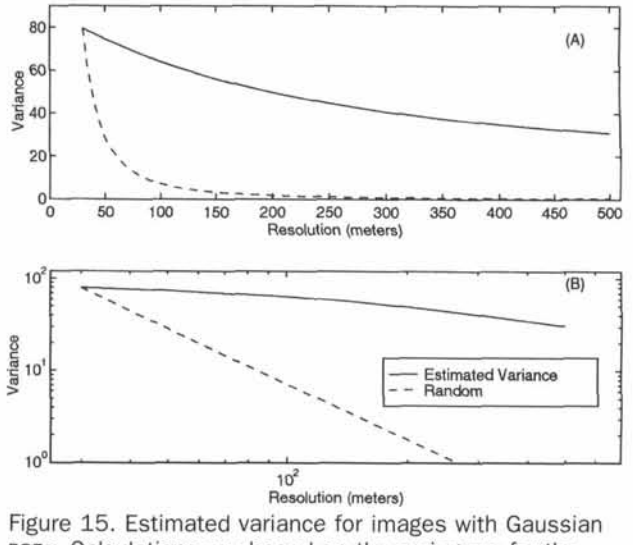

Figure 15. Estimated variance for images with Gaussian PSFs. Calculations are based on the variogram for the test image. The lower portion of the figure shows the same information as the upper portion, using logarithmic scaling.

timation of variance for spatial resolutions finer than the original data. In fact, if the punctual variogram is known, variance at *any* resolution can be determined accurately. The problem is the greater difficulty of estimating the punctual variogram from coarse data. Estimates of variance at fine scales are affected by such problems, as can be seen in Figure 6. In practice, there is no way to tell whether the punctual variogram has been estimated precisely. This uncertainty undermines confidence in fine-scale estimates made from coarse-scale data. At best, such estimates constitute reasonable guesses based on the available information, but their accuracy can not be confirmed in practice. The results presented here indicate that the quality of estimates at spatial resolutions closer to that of the original image are better than those for much finer resolutions. More experience may lead to a general rule regarding the range of resolutions over which estimates remain valid.

Comparison of the variance estimation algorithm with other approaches reveals the importance of accounting for the spatial characteristics of both the sensor and the ground scene. The existence of spatial structure in the simulated images causes the large discrepancy between the observed variances and that which would be expected in the case of random spatial structure (Figure 11). When high correlation exists between nearby values, there is less variability within pixels than between them. So image variance decreases slowly with changes in spatial resolution, resulting in higher variance than for the random case.

Aggregating blocks of pixels implicitly accounts for the spatial structure of a scene, but still does not lead to accurate variance estimation of coarse-resolution images. Interestingly, this approach corresponds to methods used in a number of studies of spatial resolution effects in remotely sensed data. Essentially, a multiresolution data set created by averaging blocks of pixels does not have the same second-order properties as one created using realistic models of sensor spatial response. The discrepancy in estimated variances is similar to that obtained by using the simpler PSF model. Both of these alternate approaches result in overestimates of variance. A probable reason is that neither accounts for overlap in the spatial response of adjacent pixels. The PSF of Landsat TM, for example, integrates some radiance from outside the nominal 30-meter instantaneous field of view (IFOV) when making a measurement (Markham, 1985). This tends to make adjacent pixel values more similar and, thus, lowers variance. Most empirical studies based on block averaging, in particular, do not take such overlap into account.

Algorithm Applicability

There are a number of important factors in the remote sensing process which are not considered in the variance estimation algorithm. The only components considered are the spatial response of the sensor, and the spatial structure of the at-sensor radiation. In some environments, viewing and illumination conditions can have a significant impact on the scene spatial structure, affecting both the magnitude and isotropy of spatial dependence. Another major factor which is not considered is the influence of the atmosphere, which can affect image variance by altering the magnitude or spatial pattern of upwelling radiation. Spatial effects induced by the atmosphere can be modeled by considering an atmospheric PSF in addition to the sensor PSF (Billingsley *et al.*, 1983). But accurate determination of the magnitude of upwelling radiances requires more detailed consideration of atmospheric constituents.

Even with a constant pattern of at-sensor radiances, actual remotely sensed images have characteristics which reduce the utility of the proposed methods. Two situations limiting the applicability of the algorithm can be identified. The first is when a shift-invariant linear system is an unsuitable model. Shift invariance implies a constant PSF for all pixels. All systems violate this assumption to some degree, due to the effects of scan angles. The magnitude of the error is small for sensors with narrower swath widths (SPOT, TM, MSS). But the suitability of the shift-invariance assumption is badly violated for some of the more synoptic sensors (e.g., AVHRR) and for most airborne sensors (e.g., TMS). Analysis of such systems could be undertaken, but the results would be limited in applicability to areas over which the PSF could be considered constant.

A second potential problem is violation of the assumptions implicit in statistical analysis of random fields, namely stationarity and ergodicity. A variogram can always be estimated from image data, but this estimation is only valid if the necessary assumptions are met. If the available image data contain major gradients in land surface characteristics (elevation, soil moisture, solar radiation, etc.), the parameters of the random field could not be regarded as stationary. Any variogram models, and conclusions drawn from them, would be invalid.

In summary, the algorithm illustrates the relationship between spatial resolution and variance, given a pattern of at-sensor radiance. The requirements of shift invariance and stationarity exclude a number of images and systems from analysis. Existing sensors differ enough in their characteristics that rarely, if ever, will a set of images be sufficiently similar that these methods can be used to determine accurately the variance of one by analysis of another. This is an unfortunate situation, but it does not render the algorithm useless. On the contrary, it is quite useful for simulation studies for examination of spatial resolution changes.

In some situations, the error arising through image processing can be related directly to the variance of the input data. Key (1994) discusses determination of accuracy of thresholding operations in estimation of the area coverage of geophysical fields. The error made in a binary classification of a remotely sensed image can be explicitly related to the variance of the cover fraction within pixels. Thus, it can be related to a description of the spatial structure of the field (i.e., the variogram) and to the spatial response of the remote sensing system.

Another application involves the assessment and correction of error in ecological process models using remotely sensed inputs. Error in such models can be related to the variance and covariance of input terms by using linearization of the statistical expectation operator (Rastetter *et al.*, 1992). Hu and Islam (1997) combine this concept with the modeling of within-pixel variance to create scale-invariant remote sensing algorithms. The approach can help determine the suitability of different sensors and different model parameterization schemes for driving physical models.

Variance is found to be estimated more precisely by using realistic models of the remote sensing process than by using simplified approaches. But it is not immediately clear how the magnitude of the errors in Figure 11 affect applied results. Sensitivity of applications to the error introduced employing simplified methods could be investigated in a future study.

Conclusion

The relationship between variance and spatial resolution of satellite images is described by a geostatistical model. The model accounts for the spatial structure of the scene using its variogram, and accounts for the sensor spatial response using the PSF. Given a satellite image and a sensor PSF, one may estimate the parameters of a punctual variogram for the underlying scene. The estimated punctual variogram may be

used to determine variance for other sensors. The algorithm performs well for simulated images. Comparison with results obtained by simpler methods indicate the importance of accounting for scene and sensor spatial properties when inferring variance at coarse resolutions.

Some complications arise if spatial structure is inferred from an actual remotely sensed image. The existence of sensor noise leads to a nugget effect in the observed variogram, which must be subtracted prior to further analysis. Also, the failure of the algorithm to account for various cross-sensor differences makes it difficult to confirm the accuracy of coarse-resolution variance estimates. Nonetheless, the methods show promise for studying the impact of sensor characteristics on the ability to retrieve land-surface parameters from remotely sensed data when employing particular processing strategies.

Acknowledgments

This research was supported by NASA grant NRA-95-MTPE-03. The authors thank Mark Friedl, David Jupp, Guido Salvucci, Jeff Key, and Alan Strahler for comments on this manuscript.

References

Atkinson, P.M., 1997. On estimating measurement error in remotely sensed images with the variogram, *International Journal of Remote Sensing*, 18(14):3075–3084.

Atkinson, P.M., and P.J. Curran, 1995. Defining an optimal size of support for remote sensing investigations, *IEEE Transactions on Geoscience and Remote Sensing*, 33(3):768–776.

Billingsley, F.C., P.E. Anuta, J.L. Carr, C.D. McGillem, D.M. Smith, and T.C. Strand, 1983. Data processing and reprocessing, *Manual of Remote Sensing* (R.N. Colwell, editor), American Society for Photogrammetry and Remote Sensing, Falls Church, Virginia, pp. 719–792.

Chou, Y.H., 1991. Map resolution and spatial autocorrelation, *Geographical Analysis*, 23(3):228–246.

Collins, J.B., and C.E. Woodcock, 1996. Explicit consideration of multiple landscape scales while selecting spatial resolutions, *Spatial Accuracy Assessment in Natural Resources and Environmental Sciences*: Second Internatinal Symposium, 21–23 May, Fort Collins, Colorado, pp. 121–128.

Cressie, N.A.C., 1985. Fitting variogram models by weighted least squares, *Mathematical Geology*, 17(5):563–586.

Curran, P.J., 1988. The semivariogram in remote sensing: An introduction, *Remote Sensing of Environment*, 37:493–507.

Cushine, J.L., 1987. The interactive effect of spatial resolution and degree of internal variability within land-cover types on classification accuracies, *International Journal of Remote Sensing*, 8(1):15–29.

Friedl, M.A., 1997. Examining the effects of sensor resolution and subpixel heterogeneity on spectral vegetation indices: Implications for biophysical modeling, *Scale in Remote Sensing and GIS* (D.A. Quattrochi and M.F. Goodchild, editors), CRC Press, Inc., Boca Raton, Florida, pp. 113–140.

Friedl, M.A., F.W. Davis, J. Michaelsen, and M.A. Morits, 1995. Scaling and uncertainty in the relationship between NDVI and land surface biophysical variables: An analysis using a scene simulation model and data from FIFE, *Remote Sensing of Environment*, 54:233–246.

Goodchild, M.F., and D.A. Quattrochi, 1997. Scale, multiscaling, remote sensing, and GIS, *Scale in Remote Sensing and GIS* (D.A. Quattrochi and M.F. Goodchild, editors), CRC Press, Inc., Boca Raton, Florida, pp. 1–12.

Hay, G.J., K.O. Niemann, and D.G. Goodenough, 1997. Spatial thresholds, image-objects, and upscaling: A multiscale evaluation, *Remote Sensing of Environment*, 62:1–19.

Hu, Z., and S. Islam, 1997. A framework for analyzing and designing scale invariant remote sensing algorithms, *IEEE Transactions on Geoscience and Remote Sensing*, 35(3):747–755.

Jenkins, G.M., and D.G. Watts, 1968. *Spectral Analysis and its Applications*, Holden-Day, Oakland, California, 525 p.

Journel, A.G., and C.J. Hiujbregts, 1978. *Mining Geostatistics*, Academic Press, London, 600 p.

Jupp, D.L.B., A.H. Strahler, and C.E. Woodcock, 1988. Autocorrelation and regularization in digital images I: Basic theory, *IEEE Transactions on Geoscience and Remote Sensing*, 26(4):463–473.

———, 1989. Autocorrelation and regularization in digital images II: Simple image models, *IEEE Transactions on Geoscience and Remote Sensing*, 27(3):247–258.

Kerekes, J.P., and D.A. Landgrebe, 1989. Simulation of optical remote sensing systems, *IEEE Transactions on Geoscience and Remote Sensing*, 27(6):762–771.

Key, J.R., 1994. The area coverage of geophysical fields as a function of sensor field-of-view, *Remote Sensing of Environment*, 48:339–346.

Marceau, D.J., P.J. Howarth, and D.J. Gratton, 1994a. Remote sensing and the measurement of geographical entities in a forested environment. 1. The scale and spatial aggregation problem, *Remote Sensing of Environment*, 49:93–104.

Marceau, D.J., D.J. Gratton, R.A. Fournier, and J. Fortin, 1994b. Remote sensing and the measurement of geographical entities in a forested environment. 2. The optimal spatial resolution, *Remote Sensing of Environment*, 49:105–117.

Markham, B.L., 1985. The Landsat sensors' spatial responses, *IEEE Transactions on Geoscience and Remote Sensing*, GE-23(6):864–875.

Markham, B.L., and J.R.G. Townshend, 1981. Land cover classification accuracy as a function of sensor spatial resolution, *Proceedings of the 15th International Symposium on Remote Sensing of Environment*, pp. 1075–1090.

Peuch, C., 1994. Thresholds of homogeneity in targets in the landscape: Relationship with remote sensing, *International Journal of Remote Sensing*, 15(12):2421–2435.

Quattrochi, D.A., and M.F. Goodchild, 1997. *Scale in Remote Sensing and GIS*, CRC Press, Boca Raton, Florida, 406 p.

Qi, Y., and J. Wu, 1996. Effects of changing spatial resolution on the results of landscape pattern analysis using spatial autocorrelation indices, *Landscape Ecology*, 11(1):39–49.

Rastetter, E.B., A.W. King, B.J. Cosby, G.M. Hornberger, R.O. O'Neill, and J.E. Hobbie, 1992. Aggregating fine-scale ecological knowledge to model coarser-scale attributes of ecosystems, *Ecological Applications*, 2(1):55–70.

Rendu, J.M., 1978. *An Introduction to Geostatistical Methods of Mineral Evaluation*, South African Institute of Mining and Metallurgy, Johannesburg, 84 p.

Rosenfeld, A., and A.C. Kak, 1982. *Digital Picture Processing*, Academic Press, New York, 457 p.

Smith, F.H., 1938. An empirical law describing heterogeneity in the yields of agricultural crops, *Journal of Agricultural Science*, 28:1–23.

Townshend, J.R.G., and C.O. Justice, 1988. Selecting the spatial resolution of satellite sensors for global monitoring of land transformations, *International Journal of Remote Sensing*, 9:187–236.

Vanmarcke, E., 1983. *Random Fields: Analysis and Synthesis*, The MIT Press, Cambridge, Massachusetts, 382 p.

Webster, R., P.J. Curran, and J.W. Munden, 1989. Spatial correlation in reflected radiation from the ground and its implications for sampling and mapping by ground-based radiometry, *Remote Sensing of Environment*, 29:67–78.

Wielicki, B.A., and L. Parker, 1992. On the determination of cloud cover from satellite sensors: The effect of sensor spatial resolution, *Journal of Geophysical Research*, 97(D12):12799–12823.

Woodcock, C.E., and A.H. Strahler, 1987. The factor of scale in remote sensing, *Remote Sensing of Environment*, 21:311–332.

Woodcock, C.E., A.H. Strahler, and D.L.B. Jupp, 1988a. The use of variograms in remote sensing: I. Scene models and simulated images, *Remote Sensing of Environment*, 25:323–348.

———, 1988b. The use of variograms in remote sensing: II. Real digital images, *Remote Sensing of Environment*, 25:349–379.

Zhang, R., A.W. Warrick, and D.E. Myers, 1990. Variance as a function of sample support size, *Mathematical Geology*, 22(1):107–121.